ACS APPLIED ELECTRONIC MATERIALS

pubs.acs.org/acsaelm Article

Nitrogen-Dependent Electronic Properties of Threading Edge Dislocations in 4H-SiC

Jiajun Li, Yazhe Wang, Ruzhong Zhu, Xiaodong Pi,* Deren Yang, and Rong Wang*

Cite This: *ACS Appl. Electron. Mater.* 2023, 5, 2664−2669 Read Online

ACCESS | Metrics & More | Article Recommendations

ABSTRACT: The dependence of the electronic properties of threading edge dislocations (TEDs) on the nitrogen (N) doping of 4H silicon carbide (4H-SiC) is investigated by combining first-principles calculations and experiments. First-principles calculations indicate that N atoms tend to accumulate at the cores of TEDs during the N doping of 4H-SiC, giving rise to the formation of TED-N complexes in N-doped 4H-SiC. The accumulation of N donors at the cores of TEDs leads to the donor-like behavior of TEDs in n-type 4H-SiC. With Kelvin probe force microscopy measurements, we verify that TEDs induce acceptor-like and donor-like states in undoped and N-doped 4H-SiC, respectively. For N-doped 4H-SiC, the resistivity decreases when the N concentration increases. In the meantime, the difference in the local Fermi energy between a TED and the perfect 4H-SiC becomes smaller, indicating that the N accumulation at the cores of TEDs may be saturated.

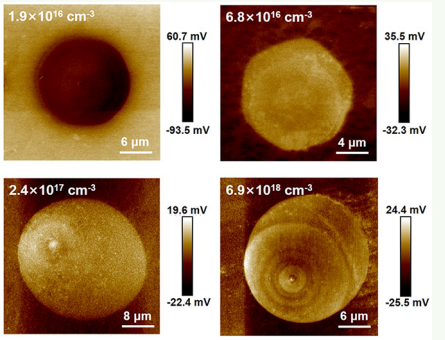

Surface potentials of TEDs with different nitrogen doping concentrations

KEYWORDS: *4H-SiC, first-principles calculations, doping, dislocations, electronic properties*

1. INTRODUCTION

4H silicon carbide (4H-SiC) has been attracting intensive attention due to its great promise for the development of high-power electronics, which features a variety of advantages such as high breakdown voltage, low power loss, and high switching speed.[1−5] It is well known that dislocations routinely appear during both the single-crystal growth and homoepitaxy of 4H-SiC. The density of threading edge dislocations (TEDs) is the highest in 4H-SiC substrates among all types of dislocations.[6,7] During the homoepitaxy of 4H-SiC, the density of TEDs increases because over 95% of TEDs are inherited from the substrates to epitaxial layers. In the meantime, over 95% of basal plane dislocations (BPDs) in the substrates are converted to TEDs during the growth of the epitaxial layers.[8,9] Given the high density of TEDs in both the substrates and epilayers of 4H-SiC, understanding the electronic properties of TEDs is critical to the applications of 4H-SiC in high-power electronics.

TEDs have been found to increase the leakage current and reduce the breakdown voltage of 4H-SiC diodes.[10−12] It was shown that the negative effect of TEDs was induced by surface pits formed by the outcrop of TEDs rather than TEDs themselves. However, a TED without a dislocation-outcrop-induced pit has been found to act as the breakdown point of a metal-oxide-semiconductor capacitor via the Shockley−Read−Hall recombination.[13,14] TEDs have also been found to narrow the Schottky barrier and increase the leakage current of a 4H-SiC diode.[15] In addition, it has been demonstrated that impurities can interplay with dislocations, affecting the electronic properties of dislocations in semiconductors.[16−19] The concentrations of nitrogen (N) in an n-type 4H-SiC epitaxial layer and an n-type 4H-SiC substrate are in the ranges of 10^{14}−10^{20} and 10^{18}−10^{19} cm^{-3}, respectively.[20] Considering the interaction between N atoms and TEDs, different N concentrations would change the electronic properties of TEDs in different layers and affect the electron transport in 4H-SiC-based power devices, especially for the vertical unipolar devices.[21,22] Therefore, discriminating the effect of the TED-related pit and the dislocation line on the electronic properties of a TED, clarifying the interaction between N and TEDs, are critical for the application of 4H-SiC in high-power electronics.

In this work, the interaction between N atoms and TEDs, as well as its effect on the electronic properties of TEDs are investigated by first-principles calculations and experimental research studies. We find that the formation energies of N at the cores of TEDs are smaller than those in the perfect region of 4H-SiC. This gives rise to the accumulation of N dopants at the cores of TEDs and thus the formation of TED-N complexes in N-doped 4H-SiC. TEDs are found to create acceptor-like states in undoped 4H-SiC. The accumulation of N donors at the cores of TEDs leads to the donor-like behavior

Received: January 31, 2023
Accepted: April 25, 2023
Published: May 5, 2023

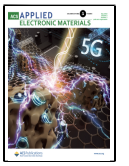

of TEDs in n-type 4H-SiC. Kelvin probe force microscopy (KPFM) measurements verify that TEDs induce acceptor-like and donor-like states in undoped and N-doped 4H-SiC, respectively. With the increase of N concentration in N-doped 4H-SiC, the resistivity decreases. Meanwhile, the difference in the local Fermi energy between TEDs and perfect 4H-SiC becomes smaller. This indicates that only when the N accumulation at the cores of TEDs are saturated, N atoms begin to substitute C atoms in the perfect region of 4H−SiC.

2. FIRST-PRINCIPLES INVESTIGATIONS

The interaction between N and TEDs and its effect on the electronic properties of TEDs are investigated by first-principles calculations. The Burgers vector of TEDs in 4H-SiC is $[11\bar{2}0]\boldsymbol{a}/3$.[23] Figure 1a presents the relaxed 4H-SiC

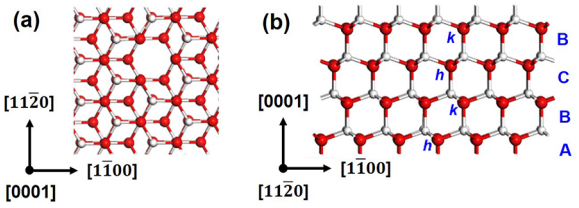

Figure 1. (a) Dislocation-core structure of a TED_{Ah} relaxed first-principles in the supercell. (b) Schematic structure of a 4H-SiC supercell with the labeled stacking sequence and inequivalent sublattice sites. The white and red balls represent C and Si atoms, respectively.

supercell containing a representative TED. To model TEDs in 4H-SiC, the *x*, *y*, and *z* axes of the supercell are reoriented along $[1\bar{1}00]$, $[11\bar{2}0]$, and $[0001]$, respectively. The TED is constructed in a 3 × 5 × 1 orthorhombic supercell, with the dimension of 16.01 Å × 15.40 Å × 10.08 Å and atomic numbers of 240 atoms. Similar to what happens in III−V compounds,[18] the dislocation core is constructed as the minimal structural model for the dislocations. Given the atomic stacking sequences of Si-C bilayers being ABCB, and sublattice sites of *h* and *k* in 4H-SiC, the individual incorporation sites for the dislocation core can be referred as the combination of Si-C bilayers and the sublattice sites, such as C*h*, B*k*, and A*h* [Figure 1b]. During the N doping of 4H-SiC, N atoms would substitute C atoms either at the core of the TED or at the perfect region located away from the TED.

First-principles calculations are carried out with projector-augmented-wave pseudopotentials as implemented in the Vienna *ab initio* simulation package (VASP),[24,25] with the plane-wave cutoff for the wavefunction expansion of 450 eV. The atomic relaxations are performed with the Perdew−Burke−Ernzerhof (PBE) exchange-correlation functional.[26] The supercell is fully relaxed until the total energy per cell and the force on each atom converge to less than 1×10^{-5} eV and 0.01 eV/Å, respectively. The Brillouin zone integration is sampled with the Γ-centered 2 × 2 × 2 Monkhorst−Pack *k*-point mesh during structural relaxations and electronic calculations.[27] Because the PBE functional significantly underestimates the band gap energies of semiconductors, the screened hybrid functional of Heyd, Scuseria, and Ernzerhof (HSE), with the fraction of the screened Fock exchange of 0.26, is then employed to calculate the electronic properties of TEDs in 4H-SiC.[28] The calculated band gap energy of 4H-SiC is 3.2 eV, which agrees well with experimental results.[29]

The formation energy of the TED with the numbers of *m* substitutional N atoms (mN_C) is calculated by

$$\Delta H_f(\mathrm{TED} - mN_C) = E_t(\mathrm{TED} - mN_C) - E_t(\mathrm{host}) + \sum n_i(\mu_i + E_i) \quad (1)$$

where $E_t(\mathrm{TED} - mN_C)$ and $E_t(\mathrm{host})$ are the total energies of the 4H-SiC supercell containing the TED−mN_C complex and the pure 4H-SiC, respectively, n_i is the number of constituent *i* (Si, C, or N) that transfers from the supercell to the reservoir during the formation of the TED, and μ_i is the chemical potential of constituent *i*, referenced to its elemental phase with energy E_i. The sum of μ_{Si} and μ_C is limited by the formation energy of the bulk 4H-SiC to maintain the host of 4H-SiC in thermal equilibrium. To avoid the elemental precipitation, the individual values of μ_{Si}, μ_C, and μ_N are limited by the total energy per atom of bulk Si, C, and N_2, respectively. The chemical potentials of N and Si are also limited by the formation energies of Si_3N_4 to prevent the formation of the secondary phase of Si_3N_4. Because the growth conditions for both the single-crystal growth and homoepitaxy of 4H-SiC are the Si-rich condition, the value of μ_{Si} of 0 eV is adopted during the formation-energy calculations in this work. We first compare the formation energies of different dislocation cores of TEDs in 4H-SiC. It turns out that the formation-energy difference among TEDs located at different atomic planes is negligible, with the formation-energy difference being smaller than 0.02 eV. The formation energy of a TED located at the *h* site is 13.85 eV, which is smaller than that located at the *k* site because less atoms are removed in this case. Therefore, we take the TED with the configuration of A*h* to investigate the interaction between N and TEDs, as well as its effect on the electronic properties of TEDs. When N atoms are incorporated at the dislocation core of a TED, N atoms can be incorporated at the A*h*, C*h*, and B*k* sites. As shown in Figure 2a, incorporation of N at the dislocation core of the TED lowers the formation energy of the TED, and the formation energy of the TED−N_{Ah} complex is the lowest. As the number of N atoms (*m*) at the core of the TED increases from 1 to 3, the formation energy of the TED−mN_C complex continuously decreases. This indicates that N prefers to accumulate at the TED cores and gives rise to the N-segregation on the TED cores during the N doping of 4H-SiC.

It has been found that both the surface relaxation effect and the long-range strain field associated with dislocation would affect the formation energy of a dislocation.[30] In order to examine the convergence of the formation energy with respect to the supercell size, we use TED_{Ah} as an example to compare the formation energies of TEDs in 3 × 5 × 1, 3 × 5 × 2, and 4 × 6 × 1 supercells by the PBE-functional calculations. The increase of the supercell size along both the *a*-/*b*-axis and *c*-axis changes the formation energies of TED_{Ah} by less than 0.06 eV. The changes in the formation energies would not change the relative stability order of TEDs in 4H-SiC. These results indicate that the 240-atom supercell is sufficient to converge defect formation energies in this work.

In order to verify the issue, we further calculate the formation energies of N_C at the supercell of 4H-SiC containing the TED by

$$\Delta H_f(mN_C) = E_t(\mathrm{TED} - mN_C) - E_t(\mathrm{TED}) + \sum n_i(\mu_i + E_i) \quad (2)$$

https://doi.org/10.1021/acsaelm.3c00137
ACS Appl. Electron. Mater. 2023, 5, 2664−2669

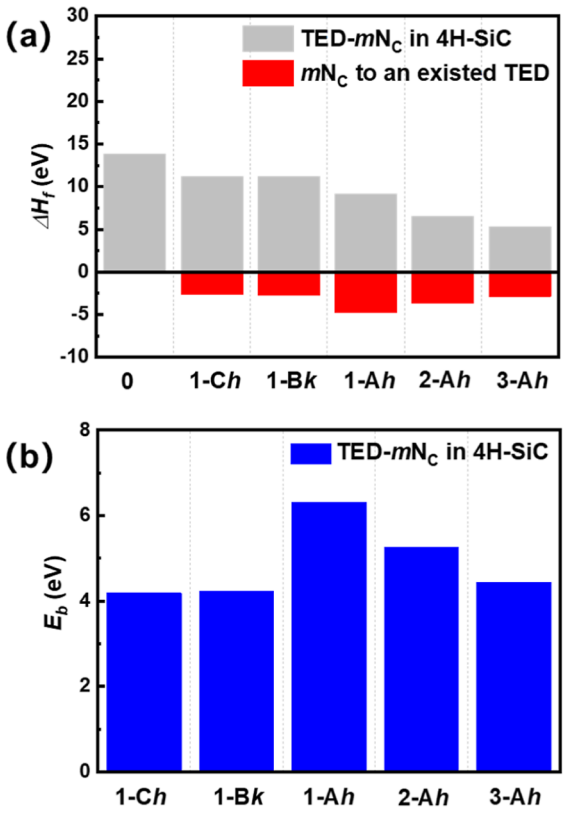

Figure 2. Calculated (a) formation energy (ΔH_f) and (b) binding energy (E_b) of the (TED−mN$_C$) complex (m = 0−3).

where E_t(TED − mN$_C$) and E_t(TED) are the total energies of the 4H-SiC supercell containing the TED−mN$_C$ complex and the 4H-SiC supercell containing the pure TED, respectively. As shown in Figure 2a, the formation energy of the TED−mN$_C$ (m = 1−3) complex is negative, indicating that the formation of the TED−mN$_C$ (m = 1−3) complex releases energy where a TED already exists. This verifies that N dopants tend to accumulate at the core of TEDs during the doping process.

The binding energies of the TED−mN$_C$ complexes [E_b(TED − mN$_C$)] are then calculated to evaluate the stabilities of the complexes by

$$E_b(\text{TED} - m\text{N}_C) = [\Delta H_f(\text{TED}) + m\Delta H_f(\text{N}_{C-\text{lattice}}) - \Delta H_f(\text{TED} - m\text{N}_C)]/m \quad (3)$$

where ΔH_f(N$_{C-\text{lattice}}$) is the formation energy of one N atom substituting one C atom in the perfect 4H-SiC lattice. As shown in Figure 2b, the values of E_b are in the range of 4.19−6.32 eV, indicating that once TED−mN$_C$ complexes are stable against decomposition once they are formed. As the number of N$_C$ accumulating at the TED core increases from 1 to 3, although the binding energy per N slightly decreases, the binding energy of the TED−3N$_{Ah}$ complex per N is still as high as 4.19 eV, which ensures the stability of the complex.

The density of states (DOSs) of the pure TED and the TED−3N$_{Ah}$ complex are then calculated. As shown in Figure 3, the TED creates localized mid-gap states and a delocalized defect state under the conduction band minimum (CBM) of 4H-SiC. In undoped 4H-SiC, the mid-gap states of TEDs behave as deep acceptor-like states. This gives rise to the decreased local Fermi energy of TEDs. During the N doping of

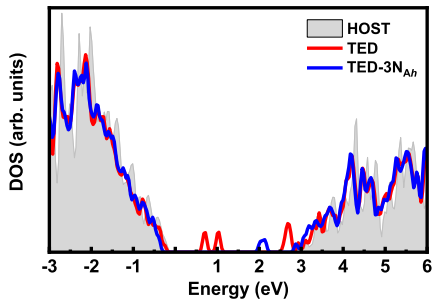

Figure 3. Calculated DOSs of the pure 4H-SiC (host), the 4H-SiC containing the TED, and the TED−3N$_{Ah}$ complex, respectively.

4H-SiC, the preference for the localization of N atoms at the cores of TEDs gives rise to the formation of TED−mN$_{Ah}$ complexes. Upon N accumulation, the mid-gap states shift to higher-energy positions in the band gap of 4H-SiC, and the defect state under the CBM disappears as a result of the electron transfer from the defect state of N$_C$ to those of the TED. The defect states at the upper-half side of the band gap could give rise to the donor-like states of TEDs in N-doped 4H-SiC.

3. EXPERIMENTAL VERIFICATIONS

In order to verify the first-principles results, we investigate the electronic properties of TEDs in 4H-SiC samples with different N-doping concentrations. 4H-SiC single-crystal boules were grown by the physical vapor transport (PVT) approach. During the PVT growth processes, the concentration of N_2 was carefully restricted. Sample A was grown without intentional nitrogen doping, while 0.1%, 1%, and 4% of nitrogen gas (N_2) were mixed into argon gas (Ar) to realize different N-doping concentrations in samples B, C, and D, respectively. After wiring sawing, lapping, and chemical mechanical polishing, 4H-SiC wafers were obtained. The N-doping concentrations of sample A were measured by the secondary ion mass spectroscopy (SIMS) (IMS 4f, Cameca). The N-doping concentrations of samples B, C, and D were calculated by the longitudinal optical plasmon coupled mode of their Raman spectra.[31,32] Raman spectra were measured by the high-resolution confocal Raman spectrometer (532 nm, LabRAM Odyssey, HORIBA). The resistivities of 4H-SiC samples were measured by contactless resistivity mapping measurement systems (Semimap COREMA-WT-150 for undoped sample A and Semilab LEI-1510EA for N-doping samples B, C, and D, respectively). The peak positions and the values of full width at half-maximum (FWHM) of (0001)-planes of the 4H-SiC wafers were measured by the X-ray diffractometer (XPert3 MRD, Malvern Panalytical). The properties of 4H-SiC samples used in this work are tabulated in Table 1.

Molten-KOH etching was carried out at 550 °C in a nickel crucible. The surface morphology of the etched samples was observed by an optical microscope (Yongxin Optics, NMM-800TRF). The depth profiles of the etch pits of TEDs were measured by the atomic force microscope (AFM) (Bruker Dimension, Edge), and the surface potentials were measured by the KPFM module equipped in the

Table 1. N-Doping Concentrations, Resistivities, and Values of FWHM of 4H-SiC Samples Used in This Work

sample	A	B	C	D
N-doping concentration (cm^{-3})	1.9 × 10^{16}	6.8 × 10^{16}	2.4 × 10^{17}	6.9 × 10^{18}
resistivity (Ω·cm)	1 × 10^{9}	13	0.2	0.019
FWHM (arcsec)	21.24	27.50	21.82	20.61

https://doi.org/10.1021/acsaelm.3c00137
ACS Appl. Electron. Mater. 2023, 5, 2664−2669

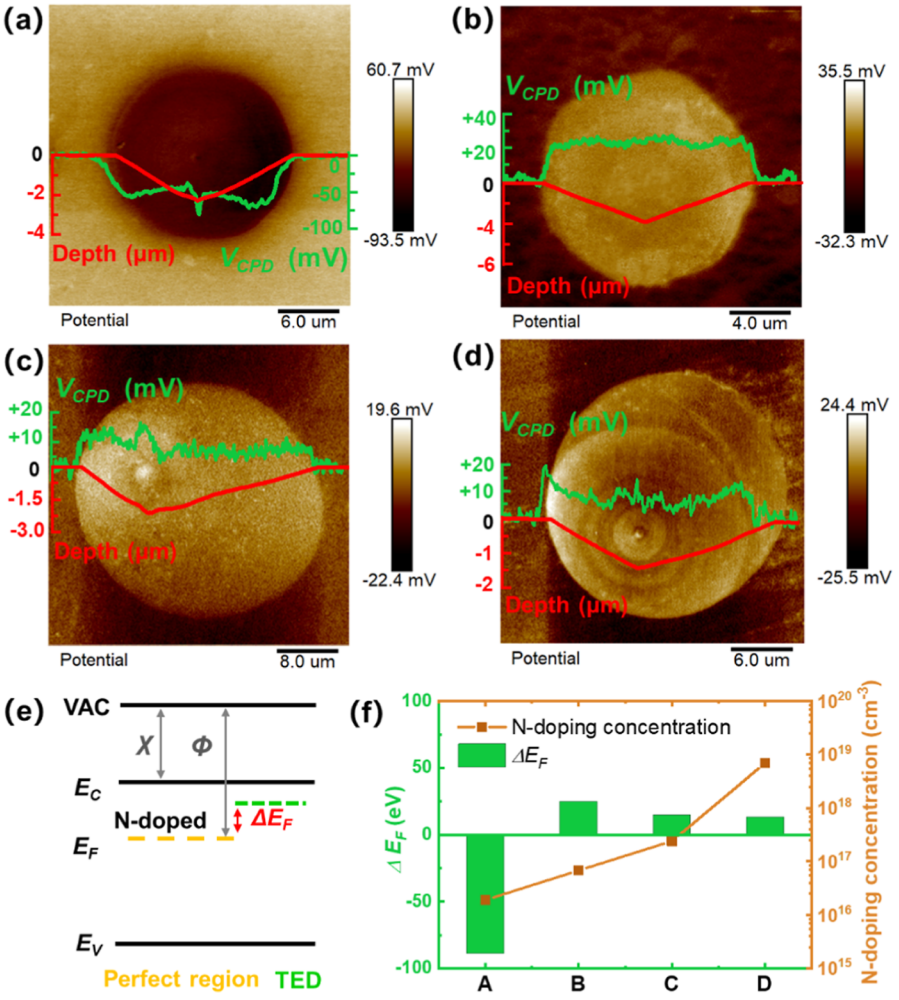

Figure 4. Surface potentials and corresponding depth profiles of representative TEDs in (a) sample A, (b) sample B, (c) sample C, and (d) sample D. (e) Band diagram of N-doped 4H-SiC containing a TED. (f) Dependence of the local Fermi energy differences (ΔE_F) between TEDs and the perfect regions around them on the doping concentrations of different 4H-SiC samples.

AFM, with a Pt−Ir coated Si cantilever. The work function of the tip is 5.5 eV.

The electronic properties of representative TEDs in 4H-SiC samples are investigated by KPFM characterizations by measuring the contact potential difference (V_{CPD}) between the TED and the TED-free region. As shown in Figure 4a, the values of V_{CPD} across the TED-related pit is lower than that of TED-free region in undoped 4H-SiC. As the N-doping concentration increases, the values of V_{CPD} across the TED-related pit becomes higher than that of the TED-free region [Figure 4b−d]. In KPFM measurements, V_{CPD} and the work function (Φ) are associated by[33]

$$V_{CPD} = (\Phi_{tip} - \Phi_{sample})/e \quad (4)$$

where $\Phi_{samplte}$ and Φ_{tip} are the work functions of the 4H-SiC sample and the Pt−Ir coated Si tip, respectively, and e is the electronic charge. The value of Φ is calculated by

$$\Phi = \chi + (E_C - E_F) \quad (5)$$

where χ, E_C, and E_F are the electron affinity, the energy of the CBM, and local Fermi energy of 4H-SiC, respectively. The relationship between the KPFM-measured V_{CPD} and the local Fermi energy of the sample is depicted in Figure 4e.

With eqs 4 and 5, the local Fermi energy differences (ΔE_F) of TEDs compared with TED-free regions can be calculated by the difference of V_{CPD} (ΔV_{CPD}) and are plotted in Figure 4f. In undoped 4H-SiC, the local Fermi energy of the TED is 88.8 meV lower than that of the TED-free region, indicating TEDs create acceptor-like defect states in undoped 4H-SiC. In N-doped 4H-SiC samples, the local Fermi energies of TEDs are always higher than those of the TED-free regions, indicating that TEDs create donor-like states in N-doped 4H-SiC. Interestingly, we find that the calculated value of ΔE_F of TEDs compared with that of the TED-free region continuously decreases with the increase of the N doping concentration of the 4H-SiC sample [Figure 4f]. According to first-principles calculations, during the N doping of sample B with the N concentration of 6.8×10^{16} cm^{-3}, N atoms tend to incorporate at the cores of TEDs, which gives rise to larger value of ΔE_F. In samples C and D, when the N concentration increases, the accumulation of N dopants at the cores of TEDs becomes saturated. The N-concentration difference between the TED core and the TED-free region becomes lower, which decreases the values of ΔE_F in samples C and D.

At last, we discuss the effect of the dependence of the electronic properties of TEDs on the N-doping concentration in the conduction mechanism of 4H-SiC power devices. Carbon vacancies (V_C) have been found to act as minority carrier lifetime killers in 4H-SiC. For 4H-SiC with low V_C density, TEDs have been found to act as carrier recombination sites, which limits the minority carrier lifetime of 4H-SiC.[34] The N concentration in the drift layer of 4H-SiC-based high-power devices varies in the range of 10^{14}−10^{16} cm^{-3} according to the requirements of high-power devices.[35] The minority carriers are holes in the N-doped drift layer. Since the electronic properties of TEDs depend on the N concentration, and N accumulation turns the acceptor-like states of TEDs to donor-like states, we propose that the

https://doi.org/10.1021/acsaelm.3c00137
ACS Appl. Electron. Mater. 2023, 5, 2664−2669

effect of TEDs on the minority carrier lifetime of 4H-SiC also depends on the N concentration. For the 4H-SiC drift layer with low N concentration, TEDs create acceptor-like states, which are capable of capturing holes and reducing the minority carrier lifetime. However, for the 4H-SiC drift layer with a high N concentration, the N accumulation turns the defects states of TEDs to donor-like states, which might not cause hole recombination and thus might not affect the minority carrier lifetime of the 4H-SiC drift layer with high N concentrations.

4. CONCLUSIONS

In conclusion, the dependence of the electronic properties of TEDs on the N-doping concentration has been revealed by first-principles calculations and experiments. First-principles calculations have indicated that N atoms tend to accumulate at the cores of TEDs during the N doping of 4H-SiC, which gives rise to the formation of TED−mN_C complexes in 4H-SiC. It has been found that TEDs create acceptor-like states in undoped 4H-SiC. Upon the accumulation of N at the cores of TEDs, the defect states of TEDs turn to be donor-like in N-doped 4H-SiC. The dependence of the electronic properties of TEDs on the N doping of 4H-SiC might affect the minority-carrier-lifetime-limiting character of TEDs in differently N-doped 4H-SiC.

AUTHOR INFORMATION

Corresponding Authors

Xiaodong Pi − *State Key Laboratory of Silicon and Advanced Semiconductor Materials & School of Materials Science and Engineering, Zhejiang University, Hangzhou, Zhejiang 310027, China; Institute of Advanced Semiconductors & Zhejiang Provincial Key Laboratory of Power Semiconductor Materials and Devices, Hangzhou Innovation Center, Zhejiang University, Hangzhou, Zhejiang 311200, China;* orcid.org/0000-0002-4233-6181; Email: xdpi@zju.edu.cn

Rong Wang − *State Key Laboratory of Silicon and Advanced Semiconductor Materials & School of Materials Science and Engineering, Zhejiang University, Hangzhou, Zhejiang 310027, China; Institute of Advanced Semiconductors & Zhejiang Provincial Key Laboratory of Power Semiconductor Materials and Devices, Hangzhou Innovation Center, Zhejiang University, Hangzhou, Zhejiang 311200, China;* orcid.org/0000-0003-3333-0180; Email: rong_wang@zju.edu.cn

Authors

Jiajun Li − *State Key Laboratory of Silicon and Advanced Semiconductor Materials & School of Materials Science and Engineering, Zhejiang University, Hangzhou, Zhejiang 310027, China; Institute of Advanced Semiconductors & Zhejiang Provincial Key Laboratory of Power Semiconductor Materials and Devices, Hangzhou Innovation Center, Zhejiang University, Hangzhou, Zhejiang 311200, China*

Yazhe Wang − *State Key Laboratory of Silicon and Advanced Semiconductor Materials & School of Materials Science and Engineering, Zhejiang University, Hangzhou, Zhejiang 310027, China; Institute of Advanced Semiconductors & Zhejiang Provincial Key Laboratory of Power Semiconductor Materials and Devices, Hangzhou Innovation Center, Zhejiang University, Hangzhou, Zhejiang 311200, China*

Ruzhong Zhu − *State Key Laboratory of Silicon and Advanced Semiconductor Materials & School of Materials Science and Engineering, Zhejiang University, Hangzhou, Zhejiang 310027, China; Institute of Advanced Semiconductors & Zhejiang Provincial Key Laboratory of Power Semiconductor Materials and Devices, Hangzhou Innovation Center, Zhejiang University, Hangzhou, Zhejiang 311200, China*

Deren Yang − *State Key Laboratory of Silicon and Advanced Semiconductor Materials & School of Materials Science and Engineering, Zhejiang University, Hangzhou, Zhejiang 310027, China; Institute of Advanced Semiconductors & Zhejiang Provincial Key Laboratory of Power Semiconductor Materials and Devices, Hangzhou Innovation Center, Zhejiang University, Hangzhou, Zhejiang 311200, China*

Complete contact information is available at: https://pubs.acs.org/10.1021/acsaelm.3c00137

Notes

The authors declare no competing financial interest.

ACKNOWLEDGMENTS

This work was supported by the National Science Foundation of China (Grant No. 62274143), "Pioneer" and "Leading Goose" R&D Program of Zhejiang (Grant Nos. 2022C01021 and 2023C01010), and the Leading Innovative and Entrepreneur Team Introduction Program of Hangzhou (No. TD2022012). Partial support was provided by the Fundamental Research Funds for the Central Universities (Grant No. 226-2022-00200) and the Natural Science Foundation of China for Innovative Research Groups (Grant No. 61721005).

REFERENCES

(1) Matsunami, H. Fundamental Research on Semiconductor SiC and Its Applications to Power Electronics. *Proc. Jpn. Acad. Ser. B Phys. Biol. Sci.* **2020**, *96*, 235−254.

(2) Benevieri, A.; Carbone, L.; Cosso, S.; Kumar, K.; Marchesoni, M.; Passalacqua, M.; Vaccaro, L. Series Architecture on Hybrid Electric Vehicles: A Review. *Energies* **2021**, *14*, 7672.

(3) Cha, K.; Kim, K. 3.3 kV 4H-SiC DMOSFET with a source-contacted dummy gate for high-frequency applications. *J. Semiconduct.* **2021**, *42*, 062801.

(4) Mishra, D. K.; Ghadi, M. J.; Li, L.; Hossain, M. J.; Zhang, J.; Ray, P. K.; Mohanty, A. A Review on Solid-State Transformer: A Breakthrough Technology for Future Smart Distribution Grids. *Int. J. Electr. Power Energy Syst.* **2021**, *133*, 107255.

(5) Wang, X.; Zhong, Y.; Pu, H.; Hu, J.; Feng, X.; Yang, G. Investigation of Lateral Spreading Current in the 4H-SiC Schottky Barrier Diode Chip. *J. Semiconduct.* **2021**, *42*, 112802.

(6) Hoshino, N.; Kamata, I.; Kanda, T.; Tokuda, Y.; Kuno, H.; Tsuchida, H. Reduction in Dislocation Densities in 4h-Sic Bulk Crystal Grown at High Growth Rate by High-Temperature Gas-Source Method. *Appl. Phys. Express* **2020**, *13*, 095502.

(7) Tsuchida, H.; Kamata, I.; Miyazawa, T.; Ito, M.; Zhang, X.; Nagano, M. Recent Advances in 4H-SiC Epitaxy for High-Voltage Power Devices. *Mater. Sci. Semicond. Process.* **2018**, *78*, 2−12.

(8) Balachandran, A.; Sudarshan, T. S.; Chandrashekhar, M. V. S. Basal Plane Dislocation Free Recombination Layers on Low-Doped Buffer Layer for Power Devices. *Cryst. Growth Des.* **2017**, *17*, 1550−1557.

(9) Myers-Ward, R. L.; VanMil, B. L.; Stahlbush, R. E.; Katz, S. L.; McCrate, J. M.; Kitt, S. A.; Eddy, C. R.; Gaskill, D. K. Turning of Basal Plane Dislocations During Epitaxial Growth on 4° Off-Axis 4H-SiC. *Mater. Sci. Forum* **2009**, *615−617*, 105−108.

(10) Grekov, A.; Zhang, Q.; Fatima, H.; Agarwal, A.; Sudarshan, T. Effect of Crystallographic Defects on the Reverse Performance of 4H-SiC JBS Diodes. *Microelectron. Reliab.* **2008**, *48*, 1664−1668.

(11) Berechman, R. A.; Skowronski, M.; Soloviev, S.; Sandvik, P. Electrical Characterization of 4H-SiC Avalanche Photodiodes Containing Threading Edge and Screw Dislocations. *J. Appl. Phys.* **2010**, *107*, 114504.
(12) Na, M.; Keum, J.; Moon, J. H.; Kang, I. H.; Bahng, W. The Effect of Threading Dislocation on Current-Voltage Characteristics of 3.3 kV 4H-SiC Schottky Barrier Diode. *ECS Trans.* **2018**, *85*, 59−65.
(13) Watanabe, T.; Hino, S.; Iwamatsu, T.; Tomohisa, S.; Yamakawa, S. Mechanism of Depletion-Mode TDDB for 4H-SiC MOS Structure. *IEEE Trans. Device Mater. Reliab.* **2017**, *17*, 163−169.
(14) Neyer, T.; Domeij, M.; Das, H.; Sunkari, S. Is There a Perfect SiC MosFETs Device on an Imperfect Crystal?. In *2021 IEEE International Reliability Physics Symposium (IRPS)*; IEEE International Reliability Physics Symposium (IRPS): Monterey, California, pp 1−6.
(15) Huang, J.-R.; Chen, T.-W.; Lee, J.-W.; Huang, C.-F.; Hong, L.-S. A Perspective on Leakage Current Induced by Threading Dislocations in 4H-SiC Schottky Barrier Diodes. *Mater. Lett.* **2022**, *310*, 131506.
(16) Luo, H.; Li, J.; Yang, G.; Zhu, R.; Zhang, Y.; Wang, R.; Yang, D.; Pi, X. Electronic and Optical Properties of Threading Dislocations in *n*-Type 4H-SiC. *ACS Appl. Electron. Mater.* **2022**, *4*, 1678−1683.
(17) Liu, X.; Zhang, J.; Xu, B.; Lu, Y.; Zhang, Y.; Wang, R.; Yang, D.; Pi, X. Deformation of 4H-SiC: The Role of Dopants. *Appl. Phys. Lett.* **2022**, *120*, 052105.
(18) Wang, R.; Tong, X.; Xu, J.; Dong, C.; Cheng, Z.; Zhang, L.; Zhang, S.; Zheng, P.; Chen, F.-X.; Zhang, Y.; et al. Acceptor Decoration of Threading Dislocations in (Al,Ga)N/GaN Heterostructures. *Phys. Rev. Appl.* **2020**, *14*, 024039.
(19) Wang, R.; Xu, J.; Zhang, S.; Zhang, Y.; Zheng, P.; Cheng, Z.; Zhang, L.; Chen, F.-X.; Tong, X.; Zhang, Y.; et al. Reducing the Reverse Leakage Current of AlGaN/GaN Heterostructures Via Low-Fluence Neutron Irradiation. *J. Mater. Chem. C* **2021**, *9*, 3177−3182.
(20) Kimoto, T. Bulk and Epitaxial Growth of Silicon Carbide. *Prog. Cryst. Growth Charact. Mater.* **2016**, *62*, 329−351.
(21) She, X.; Huang, A. Q.; Lucia, O.; Ozpineci, B. Review of Silicon Carbide Power Devices and Their Applications. *IEEE Trans. Ind. Electron.* **2017**, *64*, 8193−8205.
(22) Kimoto, T. Material Science and Device Physics in SiC Technology for High-Voltage Power Devices. *Jpn. J. Appl. Phys.* **2015**, *54*, 040103.
(23) Kimoto, T.; Cooper, J. A. *Fundamentals of Silicon Carbide Technology: Growth, Characterization, Devices, and Applications*; John Wiley & Sons, 2014.
(24) Blöchl, P. E. Projector Augmented-Wave Method. *Phys. Rev. B* **1994**, *50*, 17953−17979.
(25) Kresse, G.; Furthmüller, J. Efficiency of Ab-Initio Total Energy Calculations for Metals and Semiconductors Using a Plane-Wave Basis Set. *Comput. Mater. Sci.* **1996**, *6*, 15−50.
(26) Perdew, J. P.; Burke, K.; Ernzerhof, M. Generalized Gradient Approximation Made Simple. *Phys. Rev. Lett.* **1996**, *77*, 3865−3868.
(27) Monkhorst, H. J.; Pack, J. D. Special Points for Brillouin-Zone Integrations. *Phys. Rev. B* **1976**, *13*, 5188−5192.
(28) Heyd, J.; Scuseria, G. E.; Ernzerhof, M. Hybrid Functionals Based on a Screened Coulomb Potential. *J. Chem. Phys.* **2003**, *118*, 8207−8215.
(29) Langpoklakpam, C.; Liu, A.-C.; Chu, K.-H.; Hsu, L.-H.; Lee, W.-C.; Chen, S.-C.; Sun, C.-W.; Shih, M.-H.; Lee, K.-Y.; Kuo, H.-C. Review of Silicon Carbide Processing for Power MOSFET. *Crystals* **2022**, *12*, 245.
(30) Eshelby, J. D.; Stroh, A. N. Cxl. Dislocations in Thin Plates. *London, Edinburgh Dublin Philos. Mag. J. Sci.* **1951**, *42*, 1401−1405.
(31) Nakashima, S.; Kitamura, T.; Mitani, T.; Okumura, H.; Katsuno, M.; Ohtani, N. Raman Scattering Study of Carrier-Transport and Phonon Properties Of 4H−SiC crystals with Graded Doping. *Phys. Rev. B* **2007**, *76*, 245208.
(32) Kimoto, T.; Cooper, J. A. Appendix, A Incomplete Dopant Ionization in 4H-SiC. In *Fundamentals of Silicon Carbide Technology*; Wiley, 2014; pp 511−515.
(33) Kim, H. K.; Kim, S. I.; Kim, S.; Lee, N. S.; Shin, H. K.; Lee, C. W. Relation between Work Function and Structural Properties of Triangular Defects in 4H-SiC Epitaxial Layer: Kelvin Probe Force Microscopic and Spectroscopic Analyses. *Nanoscale* **2020**, *12*, 8216−8229.
(34) Kimoto, T.; Niwa, H.; Okuda, T.; Saito, E.; Zhao, Y.; Asada, S.; Suda, J. Carrier Lifetime and Breakdown Phenomena in SiC Power Device Material. *J. Phys. D: Appl. Phys.* **2018**, *51*, 363001.
(35) Kimoto, T.; Watanabe, H. Defect Engineering in SiC Technology for High-Voltage Power Devices. *Appl. Phys. Express* **2020**, *13*, 120101.

https://doi.org/10.1021/acsaelm.3c00137
ACS Appl. Electron. Mater. 2023, 5, 2664−2669